Electronic Supplementary Material (ESI) for ChemComm.

Supplementary Information

An unprecedented $\{Ni_{14}SiW_9\}$ hybrid polyoxometalate with high photocatalytic hydrogen evolution activity

Grégoire Paille, Amandine Boulmier, Alexandre Bensaid, Minh-Huong Ha-Thi, Thu-Trang Tran, Thomas Pino, Jérôme Marrot, Eric Rivière, Christopher H. Hendon, Olivier Oms, Maria Gomez-Mingot, Marc Fontecave, Caroline Mellot-Draznieks, Anne Dolbecq, and Pierre Mialane

Table of content:

A. Synthesis

All chemicals were provided from major chemical companies and used as received excepted $Na_{10}[A\text{-}\alpha\text{-}SiW_9O_{34}]\bullet 23H_2O$ (SiW_9)[1] and alendronic acid $H_4[O_3PC(OH)(C_3H_6NH_2)PO_3]$[2] that have been synthesized as previously described.

$Na_{12}[(\alpha\text{-}A\text{-}SiW_9O_{34})Ni^{II}_{14}(AleH)_5(Ale)_2(H_2O)_{11}(OH)_7]\cdot 80H_2O$ (**Na-SiW$_9$Ni$_{14}$Ale$_7$**). SiW_9 (500 mg, 0.17 mmol) and $NiCl_2\bullet 6H_2O$ (126 mg, 0.53 mmol) were dissolved in 10 mL of water followed by the addition of alendronic acid (70 mg, 0.28 mmol) as a solid. The pH was then quickly adjusted to 9.1 with solid sodium carbonate, and the suspension heated to 80°C for 15 min, leading to a clear yellow solution. This solution was cooled down to room temperature and after 15 min a microcrystalline yellow precipitate appeared. The microcrystalline powder was filtrated after 4 h and washed with 1M NaCl, EtOH and Et_2O (m = 64 mg, 25% based on Ni). Anal. Calcd. (found) (%) for $SiNa_{12}W_9Ni_{14}P_{14}O_{181}C_{28}N_7H_{257}$ (M. W. = 6803.1 g.mol^{-1}): C 4.94 (4.64) ; N 1.44 (1.23). EDS Calcd. (found) : Ni/W 1.55 (1.46) ; Ni/P 1.00 (0.87) ; P/W 1.55 (1.67). I.R. (cm^{-1}): 1513(m), 1395(w), 1055(s), 984(s), 931(s), 871(s), 857(s), 800(s), 668(s). Single-crystals of **Na-SiW$_9$Ni$_{14}$Ale$_7$** suitable for X-Ray diffraction have been obtained by recrystallization in a minimum amount of water. Anal. Calcd. (found) (%): C 4.94 (4.88) ; N 1.44 (1.46). EDS Calcd. (found) : Ni/W 1.55 (1.53) ; Ni/P 1.00 (0.95) ; P/W 1.55 (1.61). The I.R. spectra of the crystals and of the powder are identical.

$(P_2NC_{36}H_{30})_8Na_4[(\alpha\text{-}A\text{-}SiW_9O_{34})Ni^{II}_{14}(AleOH)_5(AleO)_2(H_2O)_{11}(OH)_7]\cdot 60H_2O$ (**P$_2$N-SiW$_9$Ni$_{14}$Ale$_7$**). Powder of **Na-SiW$_9$Ni$_{14}$Ale$_7$** (90 mg, 13.2 10^{-3} mmol) was dissolved in water at 30°C. Then, bis(triphenylphosphoranylidene)ammonium chloride (120 mg, 208 10^{-3} mmol) in 10 mL of water (pH = 8 adjusted with 0.05M NaOH, T = 30°C) was slowly added, affording a precipitate which was readily filtrated and thoroughly washed with water and dried under vacuum (m = 130 mg, 93% yield vs. **Na-SiW$_9$Ni$_{14}$Ale$_7$**). Anal. Calcd. (found) (%)

for $Na_4SiW_9Ni_{14}P_{30}O_{161}C_{316}N_{15}H_{457}$ (M. W. = 10567 g.mol^{-1}): C 35.9 (36.2); N 1.99 (1.67). EDS Calcd. (found) Ni/W 1.55 (1.43); Ni/P 0.47 (0.47); P/W 3.33 (3.05). I.R. (cm^{-1}): 1588(m), 1483(m), 1436(m), 1257(s), 1112(s), 996(m), 938(m), 882(s), 794(s), 748(s), 720(vs), 689(vs), 545(m), 530(vs), 498(s).

B. Physical characterizations

C and N elemental analyses of the solids were performed by the "Service de microanalyses ICSN CNRS", in Gif sur Yvette (France). Energy dispersive spectroscopy (EDS) measurements were performed on a JEOL JSM 5800LV apparatus. Magnetic measurements on powder were carried out with a Quantum Design SQUID Magnetometer with an applied field of 1000 G using powder samples pressed in pellets to avoid preferential orientation of the crystallites. The independence of the susceptibility value with regard to the applied field was checked at room temperature. The susceptibility data were corrected from the diamagnetic contributions as deduced by using Pascal's constant tables. FT-IR spectra were recorded in the 4000-400 cm^{-1} range on a Nicolet 30 ATR 6700 FT spectrometer. UV-vis spectra were recorded on a Perkin Elmer Lambda 750 UV/Vis/NIR spectrometer using a quartz cuvette with a 1 cm long optical pathway. Single-crystal X-Ray intensity data collections were carried out with a Bruker Nonius X8 APEX 2 diffractometer equipped with a CCD bidimensional detector using Mo Kα monochromatized radiation (λ = 0.71073 Å). The absorption corrections were based on multiple and symmetry-equivalent reflections in the data sets using the SADABS program[3] based on the method of Blessing.[4] The structure was solved by direct methods and refined by full-matrix least-squares using the SHELX-TL package.[5a] In the reported structure, there is a discrepancy between the formulae determined by elemental analysis and that deduced from the crystallographic atom list because of the difficulty in locating all the disordered water molecules and alkali ions. Disordered water molecules and

counter-ions were thus refined with partial occupancy factors. Moreover, the data set of **Na-SiW$_9$Ni$_{14}$Ale$_7$** was corrected with the program SQUEEZE,[5b] a part of the PLATON package of crystallographic software used to calculate the solvent or counterion disorder area and to remove its contribution to the overall intensity data. The hydrogen atoms were theoretically located on the basis of the conformation of the supporting atoms. The command DAMP 1500 has been used because there was some serious problem for the refinement of the position of the H15A proton, which has been found to continuously rotate around the C15 atom. The crystallographic data are gathered in Table S1. CCDC number of **Na-SiW$_9$Ni$_{14}$Ale$_7$**: 1896611.

Table S1. Crystallographic data for **Na-SiW$_9$Ni$_{14}$Ale$_7$**

Chemical formula	$C_{28}H_{210}N_7Na_{12}Ni_{14}O_{134}P_{14}SiW_9$
M_r *(g.mol^{-1})*	6004.16
Cell setting, space group	Triclinic, *P-1*
Temperature (K)	200
a, *b*, *c* (Å)	15.2253(17), 23.007(2), 29.976(7)
α, β, γ (°)	111.942(6), 90.443(7), 98.293(7)
V (Å^3)	9616.2(18)
Z	2
D_x (g cm^{-3})	2.074
Radiation type	Mo *K*α
μ (mm^{-1})	6.942
Crystal form, colour	Needles, yellow
Absorption correction	Multi-scan (based on symmetry-related measurements)
T_{min}	0.484
T_{max}	0.745
No. of measured and independent reflections	266718, 34100
Criterion for observed reflections	$I > 2\sigma(I)$
R_{int}	0.0656
No. of independent observed reflections	25967
GoF	1.029
Refinement on	F^2
R, $wR_2[F^2 > 2\sigma(F^2)]$	0.0987, 0.2471
R, wR_2 (all data)	0.1307, 0.2789
No. of parameters	1772
H-atom treatment	Constrained to parent site

[a] $R_1 = \frac{\Sigma\left|\,|F_o|-|F_c|\,\right|}{\Sigma|F_c|}$

[b] $wR_2 = \sqrt{\frac{\Sigma w(F_o^2 - F_c^2)^2}{\Sigma w(F_o^2)^2}}$

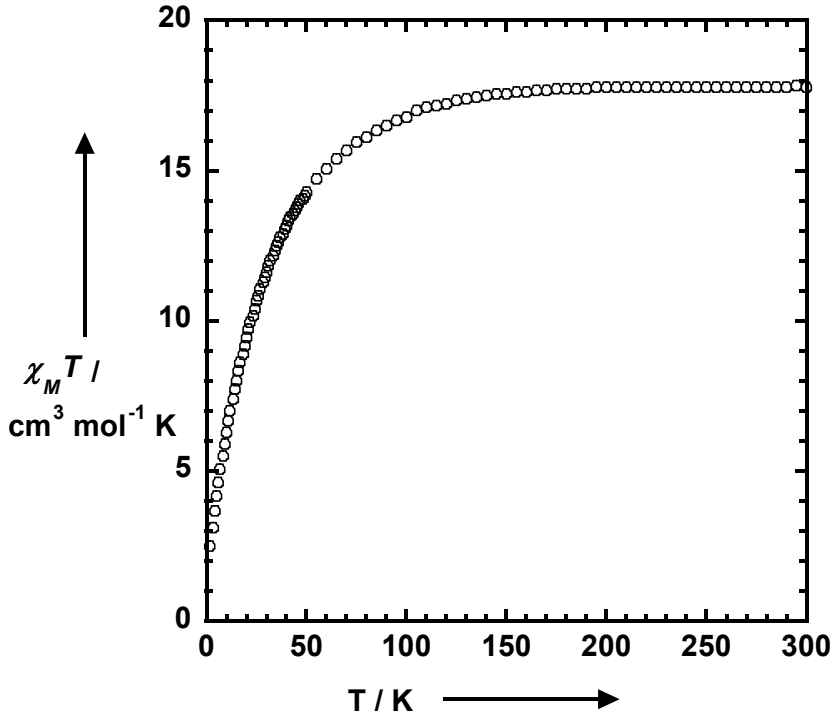

Figure S1: Thermal behaviour of $\chi_M T$ for **Na-SiW$_9$Ni$_{14}$Ale$_7$** at 1000 Oe in the 2 – 300 K range.

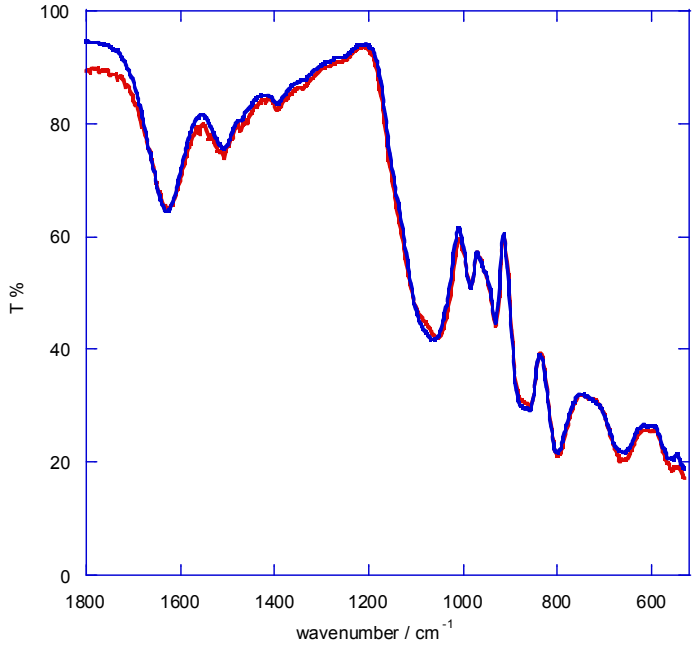

Figure S2: I.R spectra of **Na-SiW$_9$Ni$_{14}$Ale$_7$** (in red) and **Na-SiW$_9$Ni$_{14}$Ale$_7$** dissolved in water and reprecipitated with NaCl (in blue).

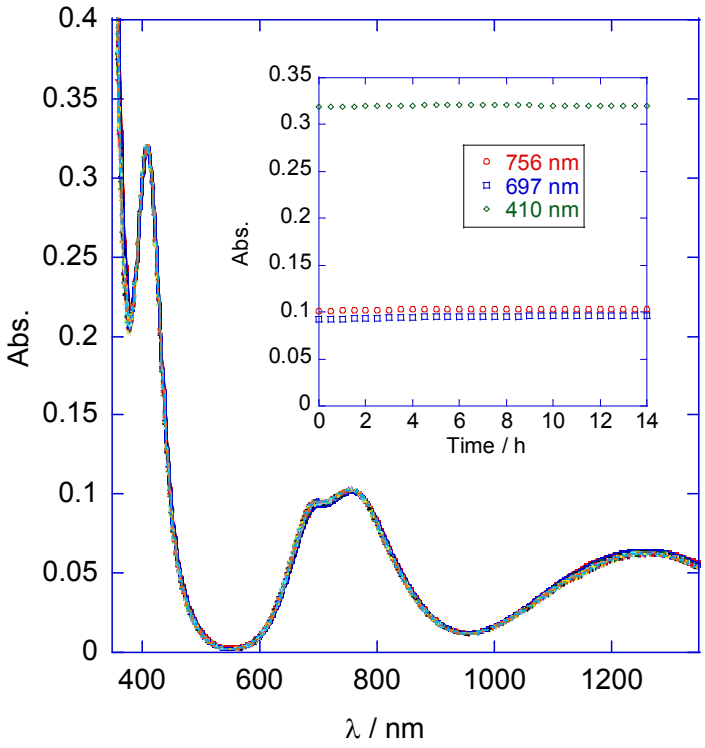

Figure S3: UV-Vis spectra of **Na-SiW$_9$Ni$_{14}$Ale$_7$** in aqueous solution ([c] = 2.10^{-3} M) recorded every hour in the 0-14 h. time range. Inset: evolution of the absorbance at 408, 697 and 761 nm in the 0-14 h. time range.

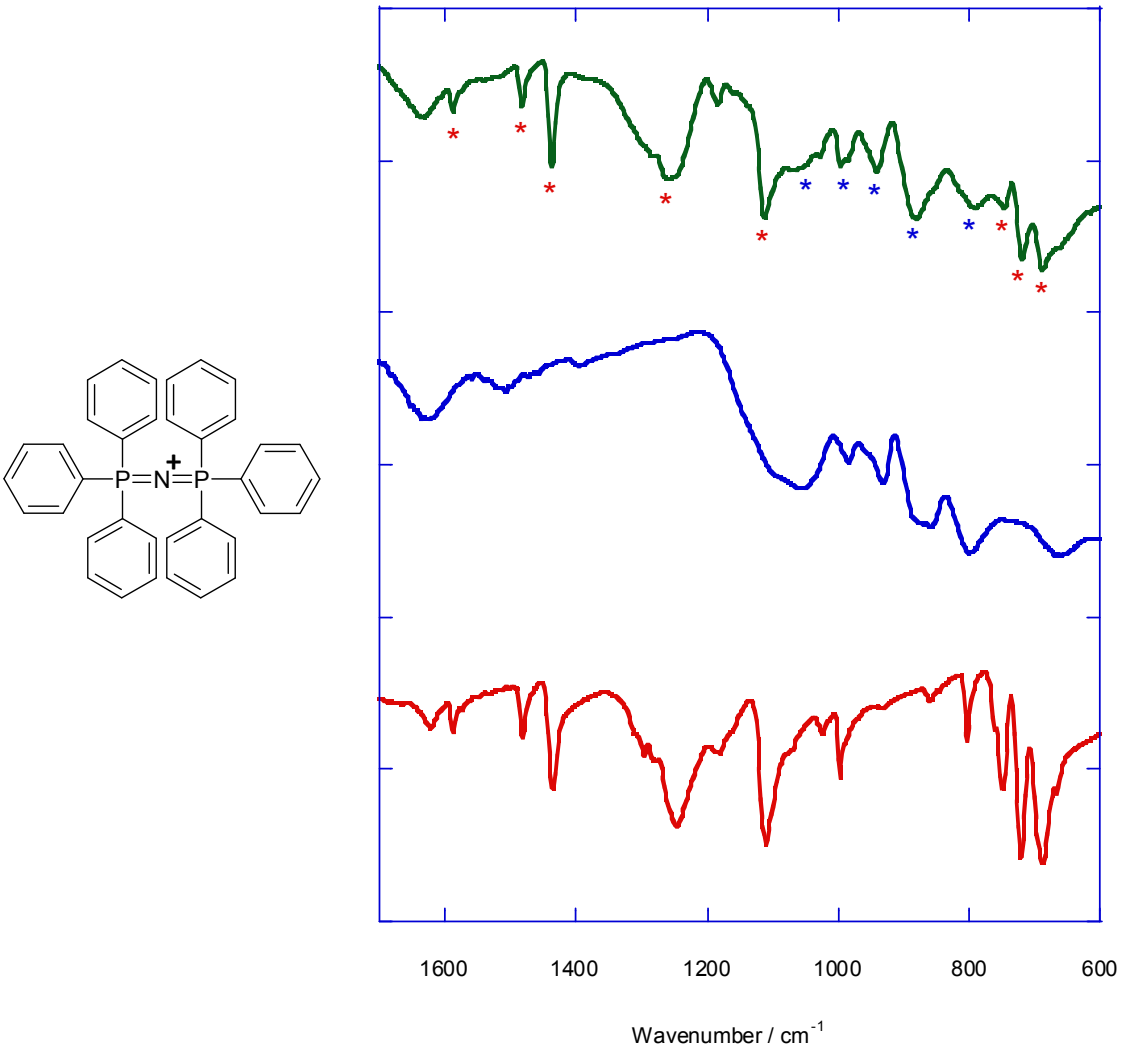

Figure S4: Left: representation of the P_2N cation; Right: I.R spectra of $(P_2N)Cl$ (red line), **Na-SiW$_9$Ni$_{14}$Ale$_7$** (blue line) and **P$_2$N-SiW$_9$Ni$_{14}$Ale$_7$** (green line). In the **P$_2$N-SiW$_9$Ni$_{14}$Ale$_7$** spectrum, the red stars refer to the bands of the P_2N countercations while the blue stars refer to those of the **Na-SiW$_9$Ni$_{14}$Ale$_7$** POM.

C. Photocatalytic experiments

All photocatalytic experiments were conducted using a 2 mL solution of 200 µM [Ir], 0.1 M BNAH and 0.25 M TEOA in acetonitrile in a 4.2 mL quartz cuvette. The cuvette is then sealed with a septum and degassed with nitrogen for 15 min in the dark, placed into a temperature controlled block at 20 °C and irradiated with a 280 W Xenon Light Source equipped with a 415 nm cut-off filter and an infrared water-filter (Asahi Spectra). During irradiation, the samples were vigorously stirred and 50 µL aliquots of the headspace were analyzed by gas chromatography analysis (Shimadzu GC-2014) with a thermal conductivity detector and a Quadrex column. H_2 measurements were quantified according to the corresponding calibration curves.

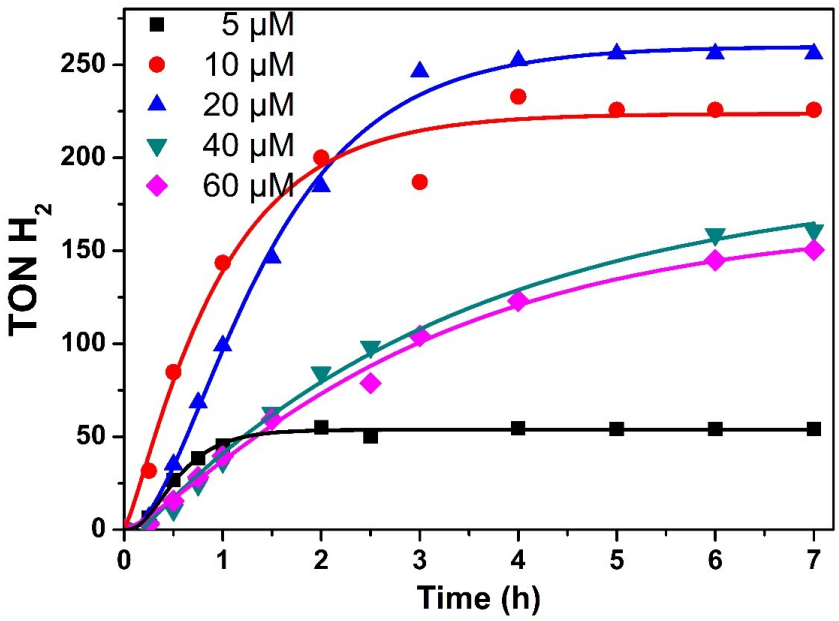

Figure S5: TON for H_2 production upon illumination at different concentrations of **P_2N-Si$W_9Ni_{14}Ale_7$**.

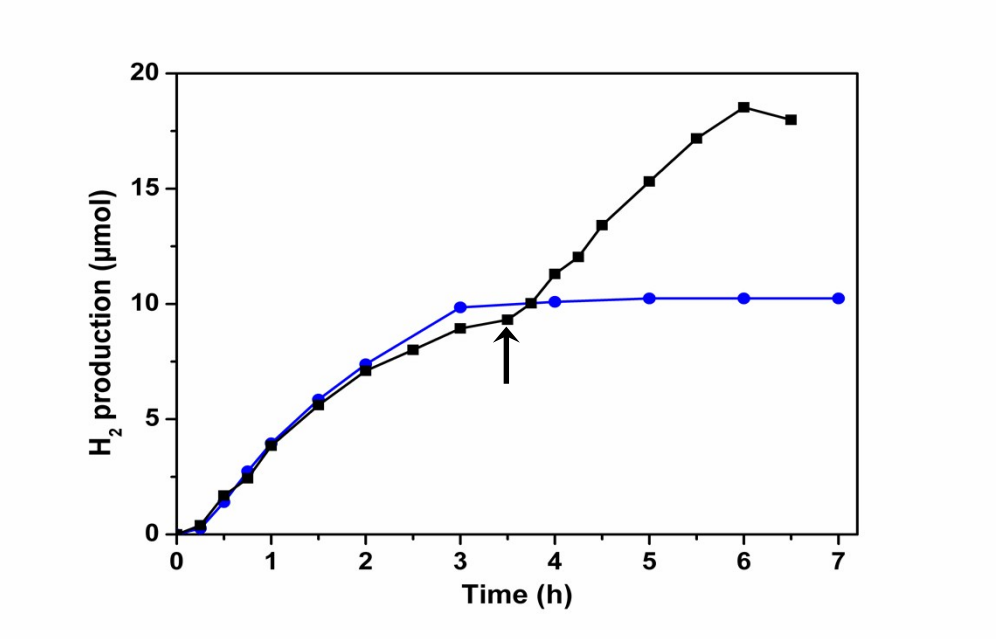

Figure S6: Hydrogen production over time of 20 µM **P_2N-$SiW_9Ni_{14}Ale_7$** (blue line). Addition of 400 nmol of [Ir] in 100 µL of CH_3CN at 3.5 hour (arrow, black curve).

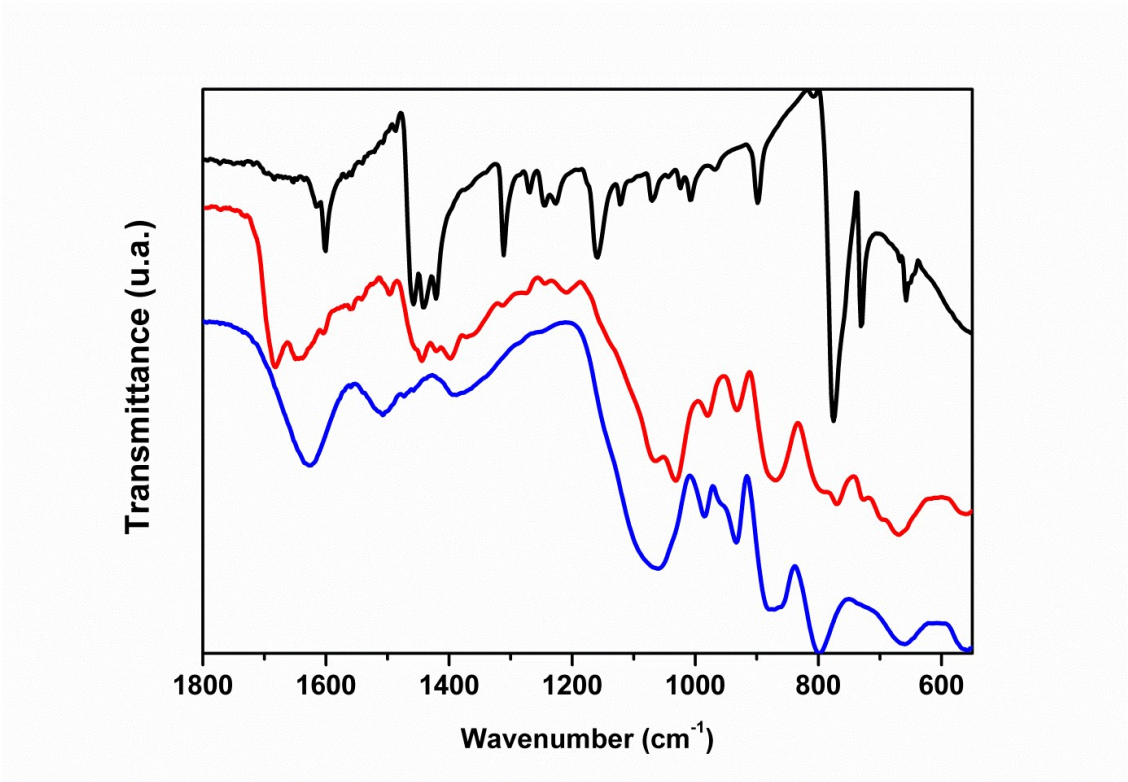

Figure S7: I.R spectra of **Na-$SiW_9Ni_{14}Ale_7$** (blue line), **$SiW_9Ni_{14}Ale_7$** precipitated after illumination for 4h in photo-catalytic conditions using an excess of $[Ru(bpy)_3]Cl_2$ (red line) and $[Ru(bpy)_3]Cl_2$ (black line).

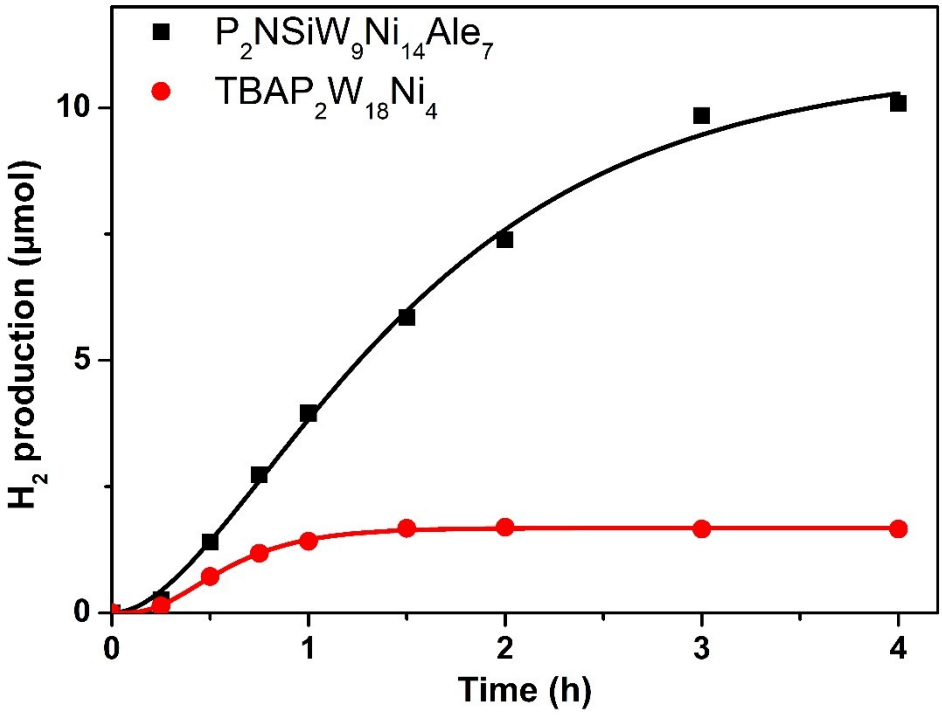

Figure S8: Comparison of H_2 production for 20 µM **P_2N-$SiW_9Ni_{14}Ale_7$** (black) and 20 µM **TBA-$P_2W_{18}Ni_4$** (red).

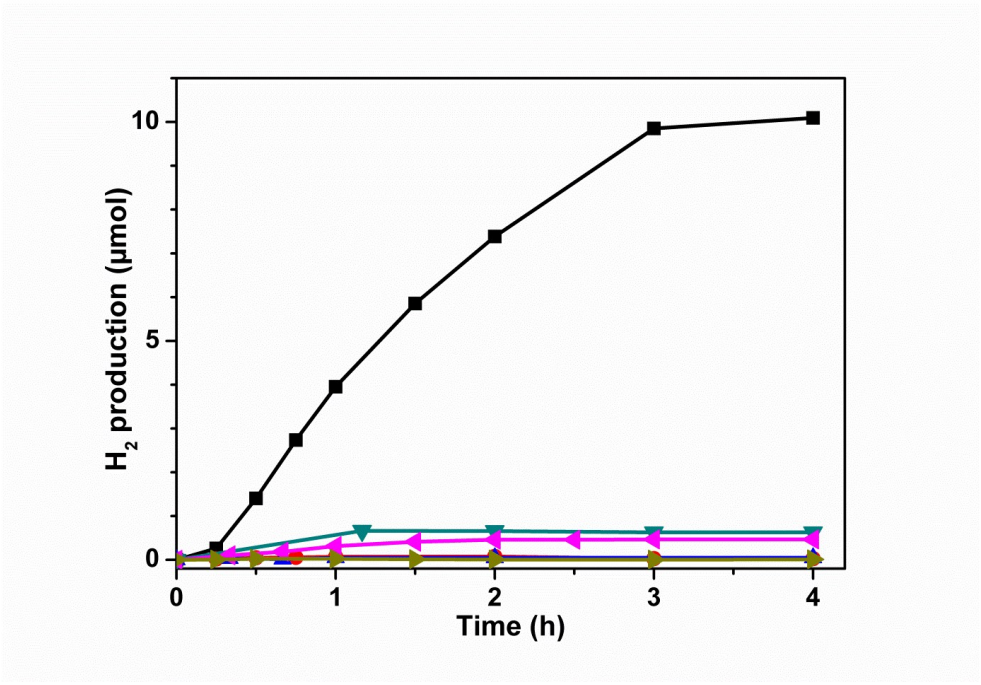

Figure S9: Control experiments for hydrogen production, at 20 µM **P_2N-$SiW_9Ni_{14}Ale_7$** (black), without **P_2N-$SiW_9Ni_{14}Ale_7$** (red), without **P_2N-$SiW_9Ni_{14}Ale_7$** nor [Ir] (blue), at 20 µM **P_2N-$SiW_9Ni_{14}Ale_7$** in the absence of BNAH (green), at 20 µM **P_2N-$SiW_9Ni_{14}Ale_7$**, 8% v/v water in the absence of BNAH (pink), at 180 µM $Ni(NO_3)_2$ (gold).

D. Electron transfer investigations

Ground state absorption spectra were measured either on a Shimazu UV-1700 or an Analytic Jena Specord spectrometer and corrected emission spectra were obtained on a Jobin-Yvon SPEX Fluoromax-4 spectrometer. Nanosecond transient absorption measurements were performed on a home-built setup which has been described previously.[6] Briefly, a Nd:YAG pumped optical parametric oscillator (OPO) laser is used for sample excitation at 430 nm with an energy of ~ 5 mJ/pulse with a repetition rate of 10Hz. After excitation the sample is probed by a white light continuum laser (LEUKOS) in a repetition rate of 20 Hz. The probe beam is split into two arms, one for probing sample and the other for reference in order to compensate for energy fluctuations. The probing arm after passing the sample is coupled into a round to linear optical fiber bundle before being analyzed by a spectrograph SPEX 270M (Jobin-Yvon). Detection of the dispersed white light is performed by an intensified CCD (ICCD) detector PIMAX 4 (Princeton Instrument). Transient absorption spectra can be calculated using the following formula:

$$\Delta OD = log_{10}\left(\frac{S_{ref}^{on}}{S_{ref}^{off}} \times \frac{S_{prob}^{off}}{S_{prob}^{on}}\right) \quad (1)$$

where S_{ref}^{on} and S_{ref}^{off} are reference spectra when pump laser is on and off respectively, S_{prob}^{on} and S_{prob}^{off} are probe spectra when pump laser is on and off respectively. Time-resolved fluorescence measurements were performed either on the same setup or on an Edinburgh Instruments LP920 Laser Flash Photolysis Spectrometer system incorporating a Continuum Q-switch Nd:YAG laser operating at 355 nm and a Continuum Surelite OPO for sample excitation (~5 ns pulse duration and energy of 7mJ at 430 nm excitation). Detection in the LP920 system is performed via a Czerny-Turner blazed 500 nm monochromator (bandwith 1-5 nm) coupled with a Hamamatsu R928 photomultiplier tube.

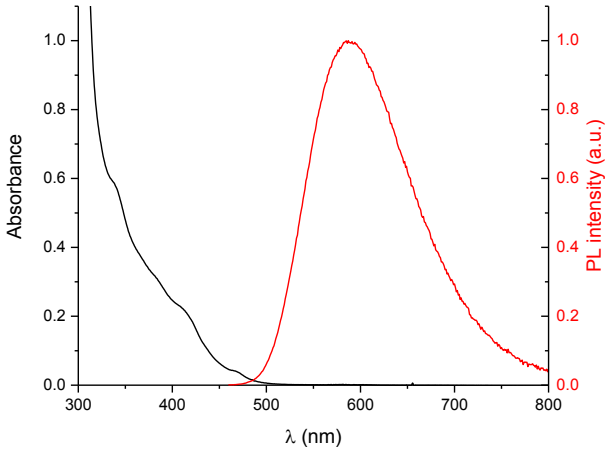

Figure S10: Absorption and photoluminescence spectra (λ_{exc} = 430 nm) of [Ir] in CH_3CN.

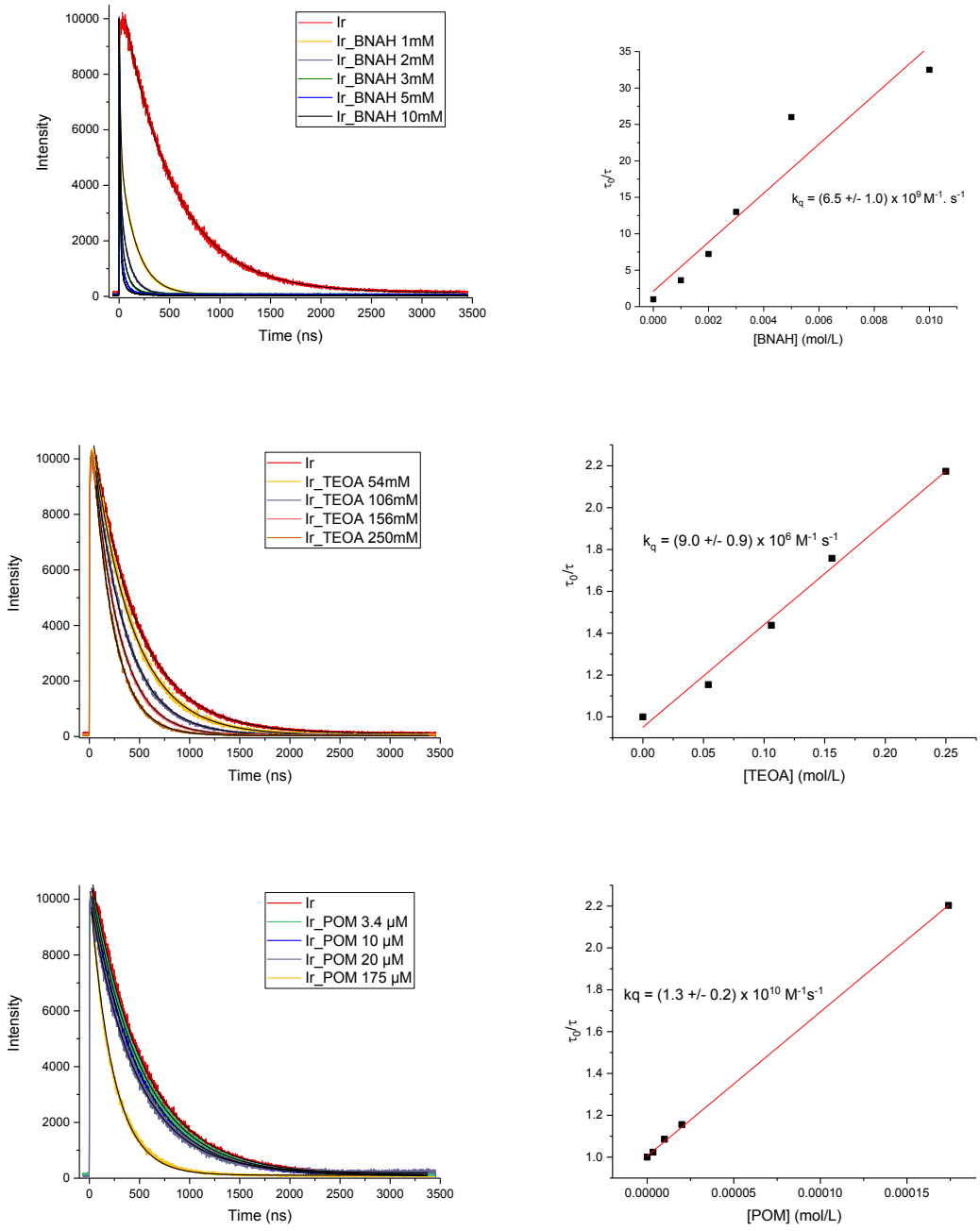

Figure S11: Photoluminescence decays at 585 nm of the [Ir] photosensitizer upon successive addition of BNAH (top), TEOA (middle) or the POM **P_2N-$SiW_9Ni_{14}Ale_7$** (bottom), with λ_{exc} = 430 nm. The concentrations of BNAH are smaller than that used in photocatalytic assay.

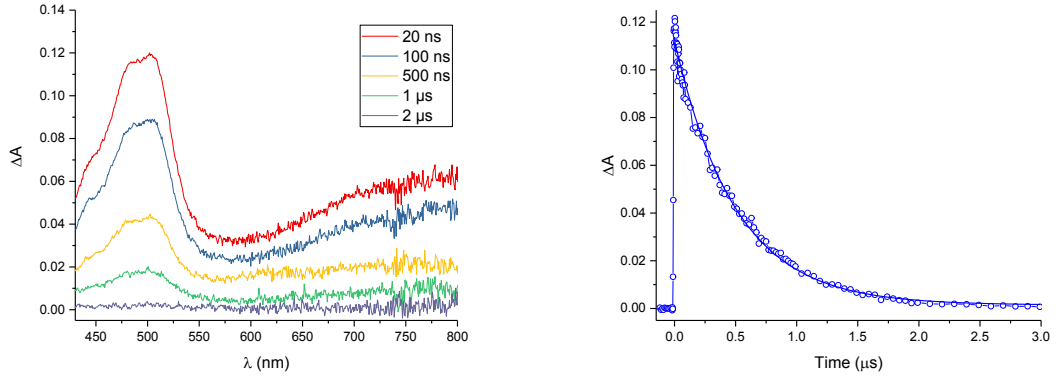

Figure S12: Transient absorption spectra and decay curve measured at 500±5 nm after excitation at 430 nm of [Ir] (200 µM) in deaerated CH_3CN.

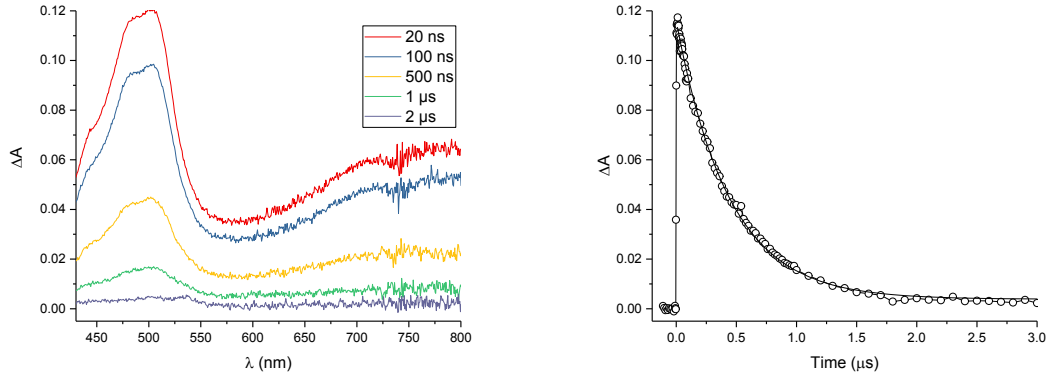

Figure S13: Transient absorption spectra and decay curve measured at 500±5 nm after excitation at 430 nm of [Ir] (200 µM) with POM **P_2N-$SiW_9Ni_{14}Ale_7$** (20 µM) in deaerated CH_3CN.

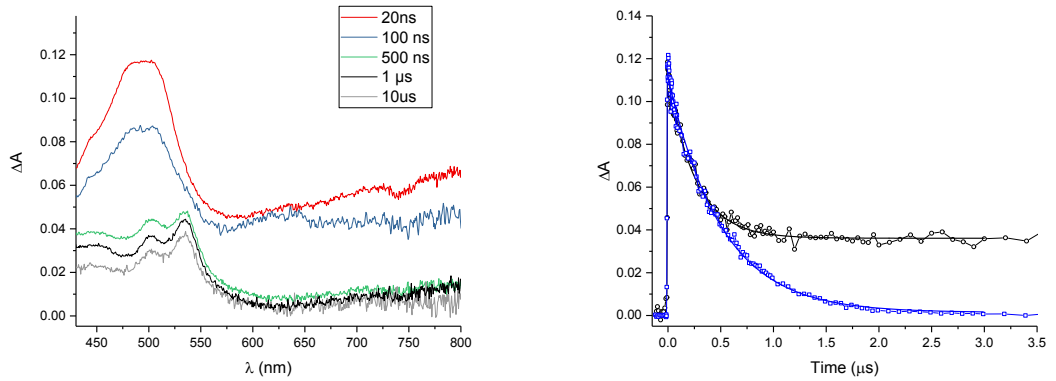

Figure S14: Transient absorption spectra and decay curves measured at 500±5 nm after excitation at 430 nm of [Ir] (200 µM) (blue curve) and [Ir] with TEOA (0.25 M) (black curve) in deaerated CH_3CN.

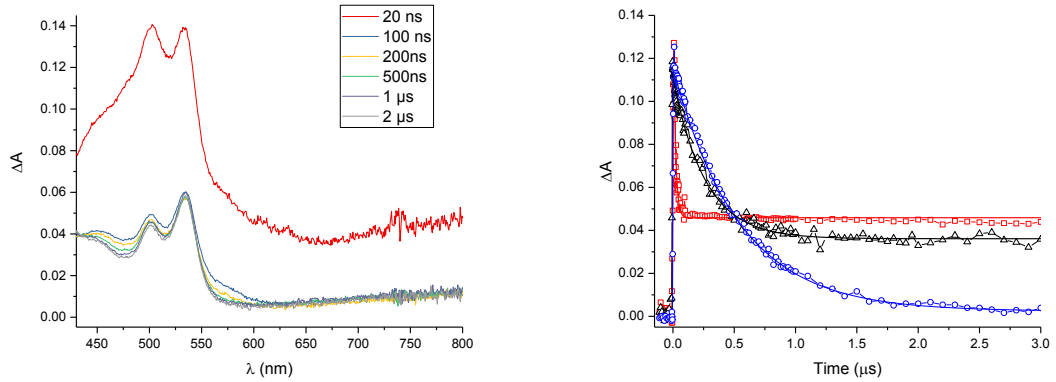

Figure S15: Transient absorption spectra and decay curves measured at 500±5 nm after excitation at 430 nm of [Ir] (200 µM) (blue curve), [Ir] with TEOA (0.25 M) (black curve) and [Ir] with BNAH (0.01 M) (red curve) in deaerated CH_3CN. The concentration of BNAH is smaller than that used in photocatalytic assay.

	k_q (M^{-1} s^{-1})	k_{app} (s^{-1})
[Ir] + BNAH	(6.5±1.0) x 10^9	(6.5±1.0) x 10^8
[Ir] + TEOA	(9 ± 0.9) x 10^6	(2.3 ± 0.3) x 10^6
[Ir] + **P_2N-$SiW_9Ni_{14}Ale_7$**	(1.3 ± 0.2) x 10^{10}	(2.6 ± 0.4) x 10^5

Table S2: Quenching rate constant k_q obtained from Stern-Volmer plot and apparent rate constant $k_{app} = k_q[Q]$ of different quenchers with their concentration used in photocatalytic conditions [BNAH] = 0.1 M, [TEOA] = 0.25 M and [**P_2N-$SiW_9Ni_{14}Ale_7$**] = 20 µM.

E. Quantum chemical simulations

Starting with the experimentally determined crystallographic structure, we attempted to find a quantum chemical minimum energy structure using PBEsol[7] and a 500 eV plane wave cutoff, as implemented in VASP,[8] a commercial software package. However due to the size of the system, even when using conservative outer-valence pseudopotentials,[9] we were unable to fully optimize the molecule due to memory restrictions. We were able to equilibrate proton positions. The electronic structure was then obtained by performing a single point calculation

using this structure, with the parameters detailed above. Due to systematic underestimation of electronic band gaps using conventional GGA,[10] the electronic structure of the POM was predicted to be metallic. While this is typically rectified by the use of a hybrid functional, we were unable to perform such a calculation because of the system size. Instead, we examined the nature of the bands at the Fermi level and found that the unoccupied states were typically localized on a hybrid of W-d and Ni-d orbitals. The frontier orbital projections were visualized using VESTA, a free software package.[11]

References

1 A. Tézé and G. Hervé, *Inorg. Synth.* 1990, **27**, 85.

2 V. Kubíček, J. Kotek, P. Hermann and I. Lukeš, *Eur. J. Inorg. Chem.* 2007, 333.

3 G. M. Sheldrick, SADABS, program for scaling and correction of area detector data, University of Göttingen, Germany, 1997.

4 R. Blessing, *Acta Crystallogr.*1995, **A51**, 33.

5 (a) G. M. Sheldrick, SHELX-TL version 5.03, Software Package for the Crystal Structure Determination, Siemens Analytical X-ray Instrument Division, Madison, WI USA, 1994; (b) P. van der Sluis and A. L. Spek, *Acta Crystallogr., Sect. A: Found. Crystallogr.*, 1990, **46**, 194.

6 S. Mendes Marinho, M.-H. Ha-Thi, V.-T. Pham, A. Quaranta, T. Pino, C. Lefumeux, T. Chamaille, W. Leibl, A. Aukauloo, *Angew. Chem. Int. Ed.* 2017, **56,** 15936.

7 J. P. Perdew, A. Ruzsinszky, G. I. Csonka, O. A. Vydrov, G. E. Scuseria, L. A. Constantin, X. Zhou, and K. Burke, *Phys. Rev. Lett.* 2008, **100**, 136406.

8 G. Kresse and J. Furthmüller, *Comput. Mater. Sci.* 1996, **6**, 15.

9 G. Kresse and J. Hafner, *J. Phys.: Condens. Matt.* 1994, **6**, 8245.

10 Fabien Tran and Peter Blaha, *Phys. Rev. Lett.* 2009, **102**, 226401.

[11] K. Momma and F. Izumi, *J. Appl. Crystallogr.* 2011, **44**, 1272-1276.